JOURNAL OF MATERIALS SCIENCE **35** (2000) 1805–1811

Phase transformations in Ti-Nb-Ta and Ti-Nb-Ta-Zr alloys

X. TANG, T. AHMED, H. J. RACK
School of Chemical and Materials Engineering, Clemson University, Clemson, SC 29634, USA
E-mail: rackh@ces.clemson.edu

Phase transformations in solution treated and quenched Ti-(13-26) Nb-(22-38) Ta (wt.%) and Ti-(13-35.5) Nb-(5-22) Ta-(4-7.2) Zr alloys have been studied. It has been observed that phase transformations in these alloys are sensitive to both composition and cooling rate. In ternary alloys, water and oil quenching resulted in the formation of orthorhombic martensite (α'') in a retained $\beta + \omega_{\text{athermal}}$ matrix, whereas slower cooling showed evidence of fine α and $\omega_{\text{isothermal}}$ formation within the β matrix. Increase of Nb + Ta content decreases the volume percentage of martensite. Moreover, addition of Zr stabilized the β phase, lowered the martensite start temperature and suppressed ω formation. Finally, dynamic moduli of air cooled quaternary alloys showed that the modulus was sensitive to the composition, a minima at Nb/Ta ratio of 12.0 and 5 at% Zr being observed, this minimum in dynamic modulus being consistent with ω phase suppression. © *2000 Kluwer Academic Publishers*

1. Introduction

Prior investigations of phase transformations in binary titanium-niobium alloys has shown that quenching from the β phase field can result in formation of two metastable martensitic structures, either hexagonal α' in alloys with Nb < 13 wt.% or orthorhombic α'' at higher Nb content [1, 2]. Additionally, at Nb contents between 24 and 50 wt.%, $\beta + \omega_{\text{isothermal}}$ or $\beta + \omega_{\text{athermal}}$ has been observed [2]. A recent study of Ti-(28–40) wt.% Nb has also shown that the α'' martensite formed in these alloys has an ordered base-centered orthorhombic crystal structure with the M_s and order-disorder temperatures being sensitive to Nb and interstitial content, decreasing with increasing Nb and O + N + C content [3].

While ternary and quaternary additions of Ta and Zr to Ti-Nb alloys have been shown to enhance the low temperature superconducting properties of these alloys [4–7], their effects on phase equilibria have not been reported. The purpose of the present work was to extend prior binary Ti-Nb phase equilibria examinations to ternary Ti-Nb-Ta and quaternary Ti-Nb-Ta-Zr alloys with emphasis being given to the influences of cooling rate and composition on phase stability.

2. Experimental procedures

Ti-Nb-Ta and Ti-Nb-Ta-Zr alloys, Table I, were arc melted as 30 g buttons from Ti (O < 240 wppm, N < 26 wppm, C: 9.9 wppm), Nb (O < 60 wppm, N: 29 wppm, C: 19 wppm, Si < 50 wppm), Zr (O < 50 wppm, N < 5 wppm, C < 30 wppm) and a Ti-77Ta master alloy (O: 270 wppm, N < 28 wppm, C < 96 wppm). Before weighing and melting, the constituents were cleaned in ethanol to remove possible surface contamination, the high purity Ti sponge being melted separately to minimize weight losses during subsequent incorporation with the Ti-77Ta master alloy, Nb and Zr. The master alloy, melted Ti, pure Nb and Zr were weighed within ±0.0005 g, subsequent melting being carried out in a high purity (1 wppb) argon atmospher, water cooled copper hearth non-consumable tungsten electrode arc furnace. Prior to melting, a titanium getter was also melted in the furnace which had been evacuated and flushed three times with purified argon. The alloys were melted at least five times, each time being held in the molten state for 2–3 minutes, the button being flipped between each melt. After melting alloys were reweighed, the percentage weight loss being observed to vary between 0.4 to 1.3%.

Following solidification, the ends of the cast buttons were removed, the rest of the buttons cleaned with ethanol and wrapped in tantalum foil. These were then encapsulated in quartz tubes together with a small quantity of titanium sponge under a 25 torr partial pressure of high purity argon and homogenized at 900°C for 96 hrs followed by furnace cooling. Finally, the homogenized samples were re-encapsulated and solution treated at 1000°C for 2 hours followed by water quenching, oil or air cooling, respectively.

Characterization of the resulting microstructure involved room temperature x-ray diffraction, optical and transmission electron microscopy. Room temperature x-ray diffraction analysis was carried out with Cu K_α radiation at 40 kV and 30 mA, the scanning rate being 5° 2θ/min from $2\theta = 20°$ to 80°. Following data

TABLE I Chemical compositions[a] of Ti-Nb-Ta-(Zr) alloys

Alloy	Nominal content (wt%)	Analyzed contents (wt%)	O ppm	N ppm	C ppm	Tot. int.
TA1	Ti-26Nb-22Ta	Ti-25.0Nb-21.9Ta	540	30	85	655
TA2	Ti-24Nb-22Ta	Ti-23.2Nb-22Ta	460	30	90	580
TA3	Ti-14.5Nb-38Ta	Ti-14.0Nb-37.6Ta	540	50	110	700
TA4	Ti-13Nb-38Ta	Ti-12.7Nb-38.5Ta	460	20	65	545
TA5	Ti-24Nb-22Ta-4.5Zr	Ti-23.8Nb-21.6Ta-4.6Zr	460	50	100	610
TA6	Ti-22Nb-22Ta-4.0Zr	Ti-22.2Nb-22.2Ta-4.1Zr	390	70	30	490
TA7	Ti-29Nb-12.5Ta-7Zr	Ti-29.2Nb-12.4Ta-7.1Zr	390	20	60	470
TA8	Ti-35.5Nb-5Ta-7Zr	Ti-35.5Nb-5.0Ta-6.9Zr	380	20	70	470
TA9	Ti-35.1Nb-5.7Ta-7.2Nb	Ti-35.3Nb-5.7Ta-7.3Zr	370	70	40	480

[a]Determined following homogenization. Tot. Int.: Total Interstitial = O + N + C.

collection, lattice parameter determination and peak indexing utilized a least square iterative method [8].

The homogenized and solution treated alloys were also prepared for optical microscopy by either mechanical polishing or electropolishing, the latter with a solution of 300 ml methanol, 180 ml n-butanol and 30 ml perchloric acid at a voltage and temperature of 20 V and $\leq 10^{\circ}$C respectively. Finally, the samples were etched with 8 vol% HF, 15 vol% HNO_3 and 77 vol% H_2O. Samples for transmission electron microscopy were prepared by mechanical waffering, grinding to 0.15 mm thickness and electropolishing in a solution of 5 vol% H_2SO_4, 2 vol% HF and 93 vol% methanol at 15 to 20 volts and $\leq -40^{\circ}$C.

Mechanical characterization of solution treated Ti-Nb-Ta and Ti-Nb-Ta-Zr included microhardness and dynamic modulus measurements. The former was conducted with a 200 g load on a pre-polished sample, an average of ten readings with an error of ± 5 VHN being reported. Dynamic moduli were determined with 5 mm cube samples obtained from solution treated and air cooled quaternary alloys. Standard through-transmission techniques were utilized with wet coupled (glycerine and honey) longitudinal and shear transducers having active diameters of 6.35 mm and 3.17 mm operating at frequencies of 5 MHz and 2 MHz respectively. Longitudinal (V_l) and shear (V_t) velocities were calibrated with measurements of pure Al (99.9999), Young's modulus, E, and Poisson's ratio, ν, then being given by:

$$E = V_l^2 \cdot \rho \cdot (1+\nu) \cdot (1-2\nu)/(1-\nu)$$

$$\nu = (1-2b^2)/(2-2b^2),$$

where $b = V_t/V_l$ and $\rho =$ the alloy density.

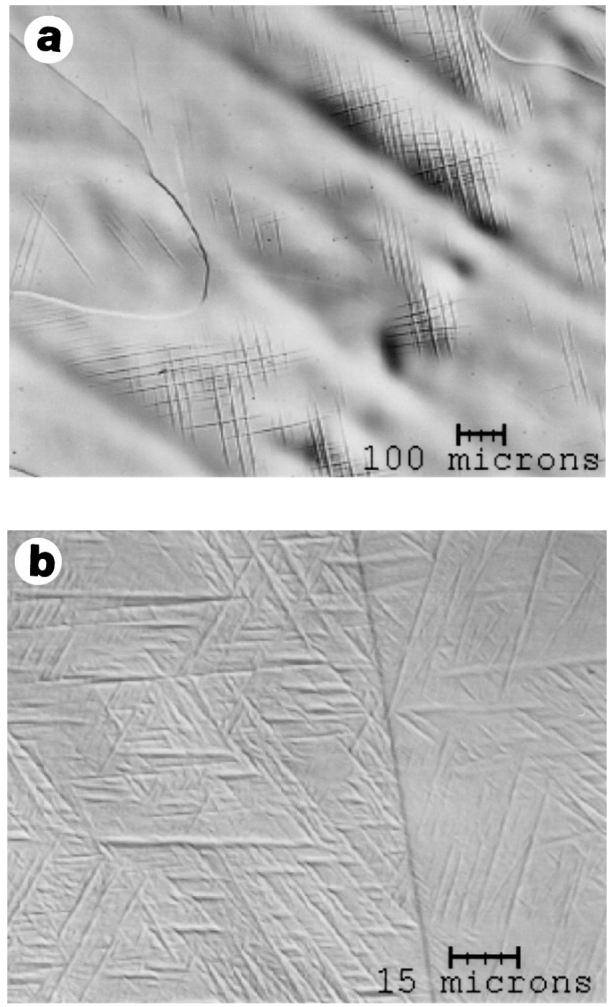

Figure 1 Representative solution treated and water quenched microstructure (a) TA2 and (b) TA5 (Nomarski interference).

3. Results

The importance of cooling rate composition on phase equilibria in Ti-Nb-Ta and Ti-Nb-Ta-Zr alloys was examined by solution treating at 1000°C for 2 hrs followed by air, oil or water quenching. In addition, the microstructure of these alloys furnace cooled after homogenization was examined. Water and oil quenching of TA1–TA6 resulted in a martensite transformation, see for example TA2 shown in Fig. 1a. The volume fraction of martensite decreased either by increasing Nb + Ta content or with addition of Zr, this later decrease being evidenced by comparison of water quenched TA5, Fig. 1b. Room temperature x-ray diffraction analysis indicated that the martensite had an orthorhombic crystal structure with lattice parameters $a = 0.316$ nm, $b = 0.482$ nm and $c = 0.462$ nm.

Optically, the martensite phase consisted of long and relatively thick primary plates with fine secondary plates in areas contained between the primary plates. Transmission electron microscopy showed that the martensitic plates had an acicular morphology with a substructure comprised of stacking faults, arrowed

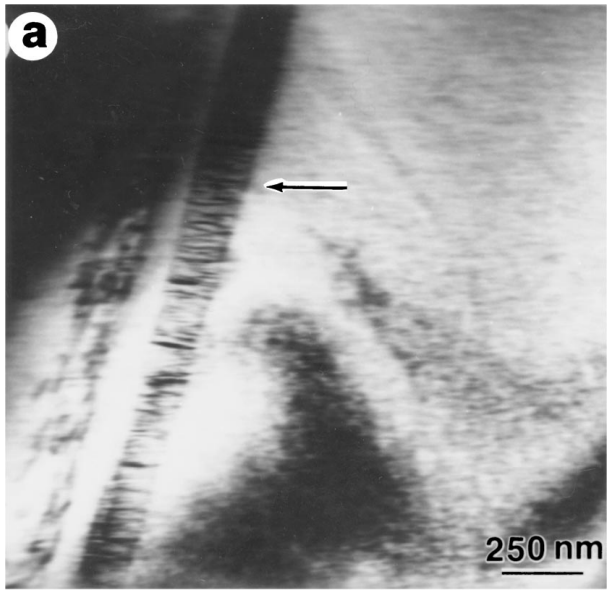

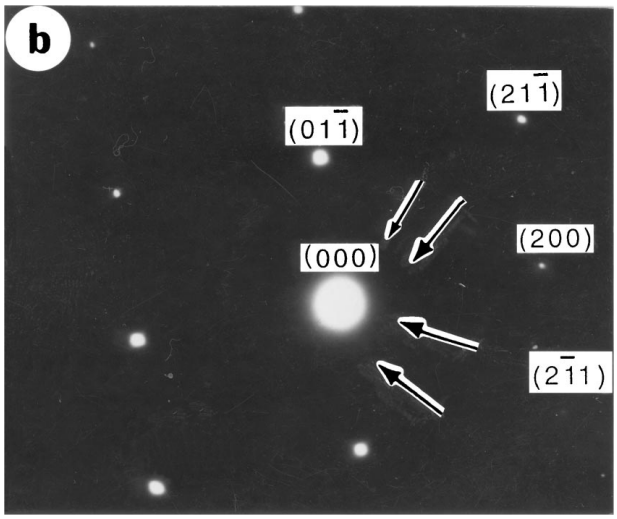

Figure 2 (a) Bright field TEM micrograph of solution treated and water quenched alloy TA2 showing martensitic plates in β matrix. (b) SAD pattern from the β matrix showing diffuse ω reflections, $g = [011]_\beta$.

in Fig. 2a. No evidence of ordering was observed within these martensitic plates, consistent with their high Nb + Ta content as compared to the prior study of binary Ti-Nb [3]. Some streaking was also seen in the SAD pattern of the retained β matrix, Fig. 2b, an indication of the early stage of the ω formation. Since this ω phase was formed during continuous water quenching, it is very similar to the athermal ω phase reported by Duerig *et al*. [9] and will be denoted ω_{ath} hereafter. In this condition, no ω phase images could be obtained. Similar streaking due to ω_{ath} formation was also observed in TA7 through TA9 alloys after water and oil quenching although optically these alloys appeared to be single phase β.

Following air cooling, TA1–TA4 appeared by optical microscopy to be single phase β, for example TA1 in Fig. 3. Again, however, more detailed transmission electron microscopy of solution treated and air cooled TA1–TA4 indicated the presence of fine α plus ω particles within the β matrix, Fig. 4a. The presence of

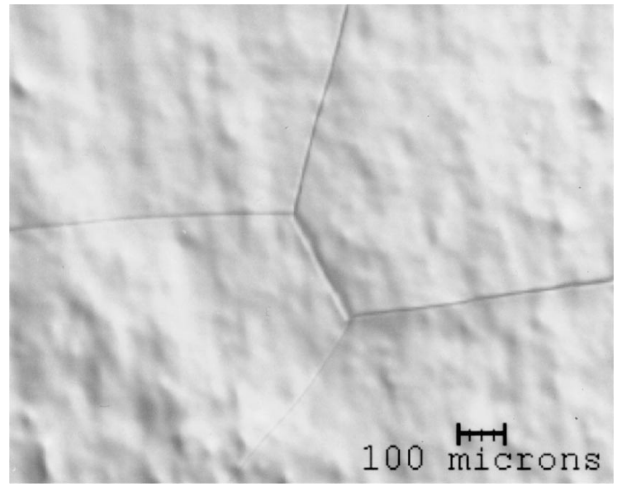

Figure 3 Representative solution treated and air cooled microstructure of TA1 (Nomarski interference).

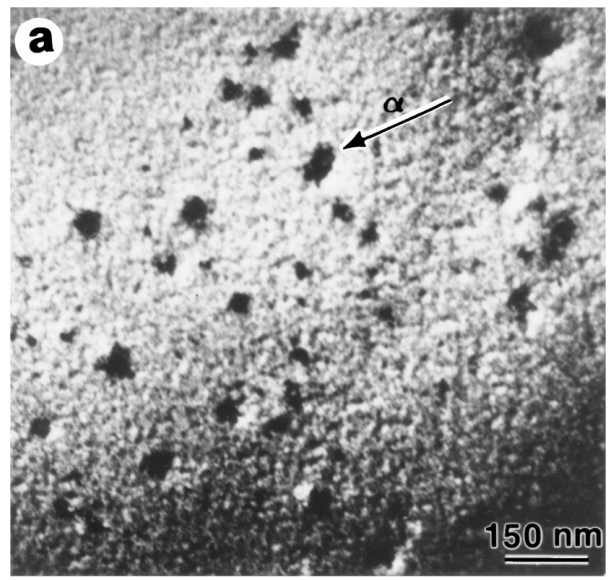

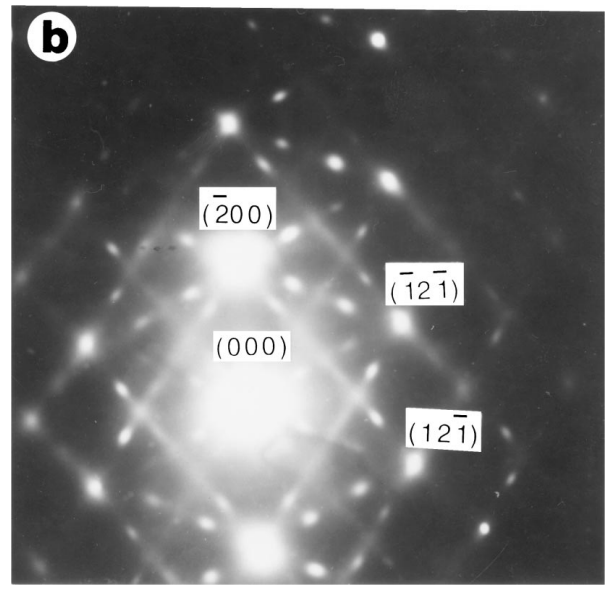

Figure 4 (a) Bright field TEM micrograph of solution treated and air cooled TA2 alloy showing fine particles. (b) SAD pattern showing ω diffractions, $g = [012]_\beta$.

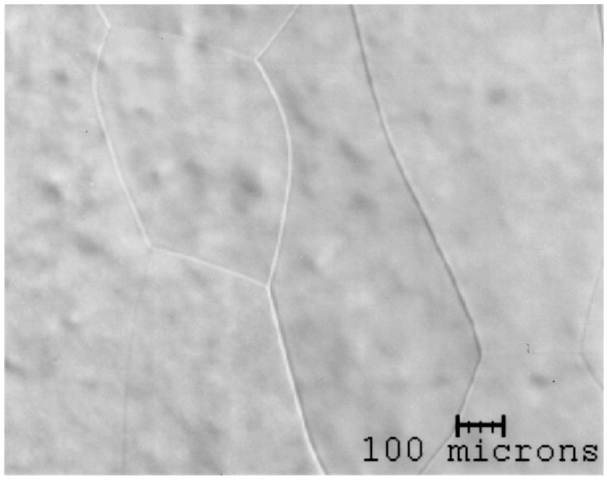

Figure 5 Optical microstructure of TA9 after solution treating and air cooling (Nomarski interference).

ω under these cooling conditions was confirmed by diffraction analysis, Fig. 4b. The strong ω reflections shown in Fig. 4b, indicated that the development of the ω phase has significantly progressed during slower air cooling. Indeed, this phase development is similar to the isothermal ω phase reported by Duerig *et al*. [9] and will therefore be henceforth denoted as ω_{iso}. Again, addition of Nb, Ta and Zr tended to stabilize the β phase, a $\beta + \omega_{ath}$ microstructure being observed following air cooling, Fig. 5.

Finally, optical microscopy of furnace cooled TA1 through TA4 showed that these samples consisted of large β grains with intra and intergranular α, increasing Nb + Ta content and Zr addition decreasing the volume fraction of α, Fig. 6. Transmission electron microscopy, Fig. 7a and b, indicated that at the highest Nb, Ta and Zr contents, the microstructure was $\beta + \omega_{iso}$.

The microhardness of homogenized and solution treated alloys are given in Table II. The hardness values of the homogenized alloys show a decrease with increasing Nb content at constant Ta and Zr. Further, the hardness of solution treated and air cooled samples TA1 to TA3 are similar to values obtained after homogenization, whereas TA4 to TA9 have lower values. Following oil and water quenching, TA1 through TA4 have lower hardness than obtained after air cooling whereas TA5 through TA9 have similar hardness independent of cooling rates.

TABLE II Microhardness of Ti-Nb-Ta-(Zr) alloys

Alloy	Analyzed contents (wt%)	VHN homog	VHN ST1000		
			AC	OQ	WQ
TA1	Ti-25.0Nb-21.9Ta	198	193	152	147
TA2	Ti-23.2Nb-22.0Ta	216	210	149	147
TA3	Ti-14.0Nb-37.6Ta	215	210	168	166
TA4	Ti-12.7Nb-38.5Ta	252	197	158	161
TA5	Ti-23.8Nb-21.6Ta-4.6Zr	197	164	155	150
TA6	Ti-22.2Nb-22.2Ta-4.1Zr	223	157	152	146
TA7	Ti-29.2Nb-12.4Ta-7.1Zr	193	167	160	151
TA8	Ti-35.5Nb-5.0Ta-6.9Zr	189	151	145	139
TA9	Ti-35.3Nb-5.7Ta-7.3Zr	195	153	150	146

Homo: Homogenized-900°C-96 hr-furnace cooled; ST1000: Solution treated-1000°C-2 hr; AC: Air cooled; OQ: Oil quenched; WQ: Water quenched.

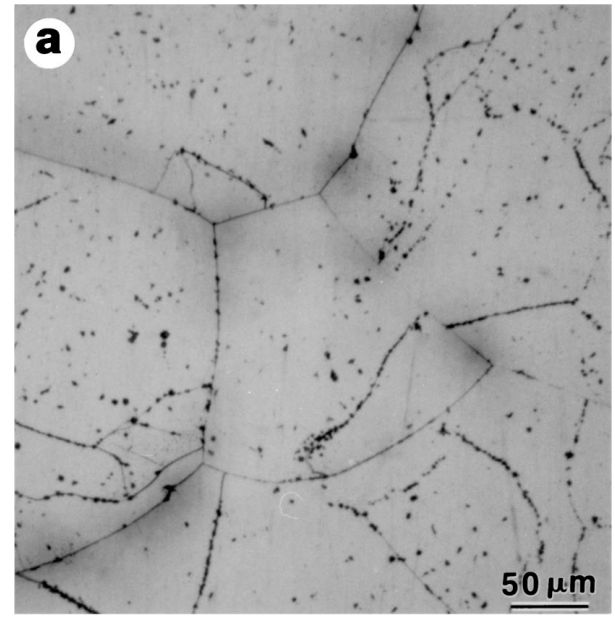

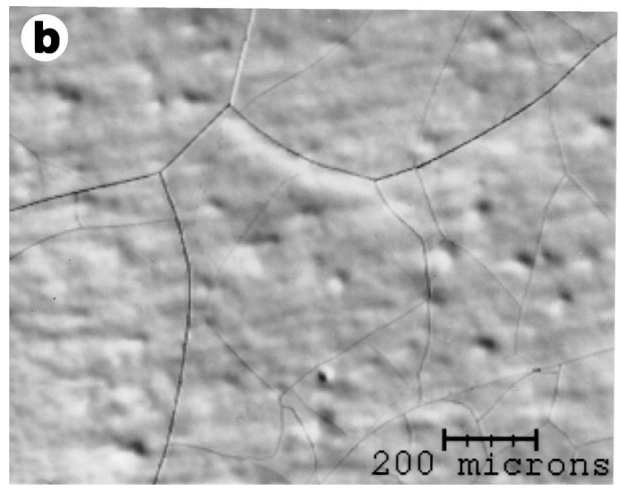

Figure 6 Representative homogenized and furnace cooled microstructure (a) TA3 and (b) TA6 (Nomarski interference).

Dynamic moduli results, Table III, show that quaternary Ti-Nb-Ta-Zr alloys have very low dynamic modulus when compared to conventional titanium alloys. These observations also indicate that the dynamic moduli of Ti-Nb-Ta-(Zr) alloys are extremely sensitive to composition, slight variations in the composition (or Nb/Ta ratio in at%) causing an appreciable variation in modulus.

TABLE III Values of dynamic modulus of Ti-Nb-Ta-Zr alloys

Alloy	Analyzed content (at%)	Nb + Ta	Dynamic modulus GPa ± 10%	Density (g/cm^3)
TA5	Ti-17.4Nb-8.1Ta-3.4Zr	25.5	55.3	6.23
TA6	Ti-16.1Nb-8.2Ta-3.4Zr	24.3	64.9	6.19
TA7	Ti-20.5Nb-4.5Ta-5.1Zr	25.0	50.0	5.23
TA8	Ti-24.1Nb-1.7Ta-5.0Zr	25.8	55.7	5.74
TA9	Ti-24.2Nb-2.0Ta-5.1Zr	26.2	48.0	5.85

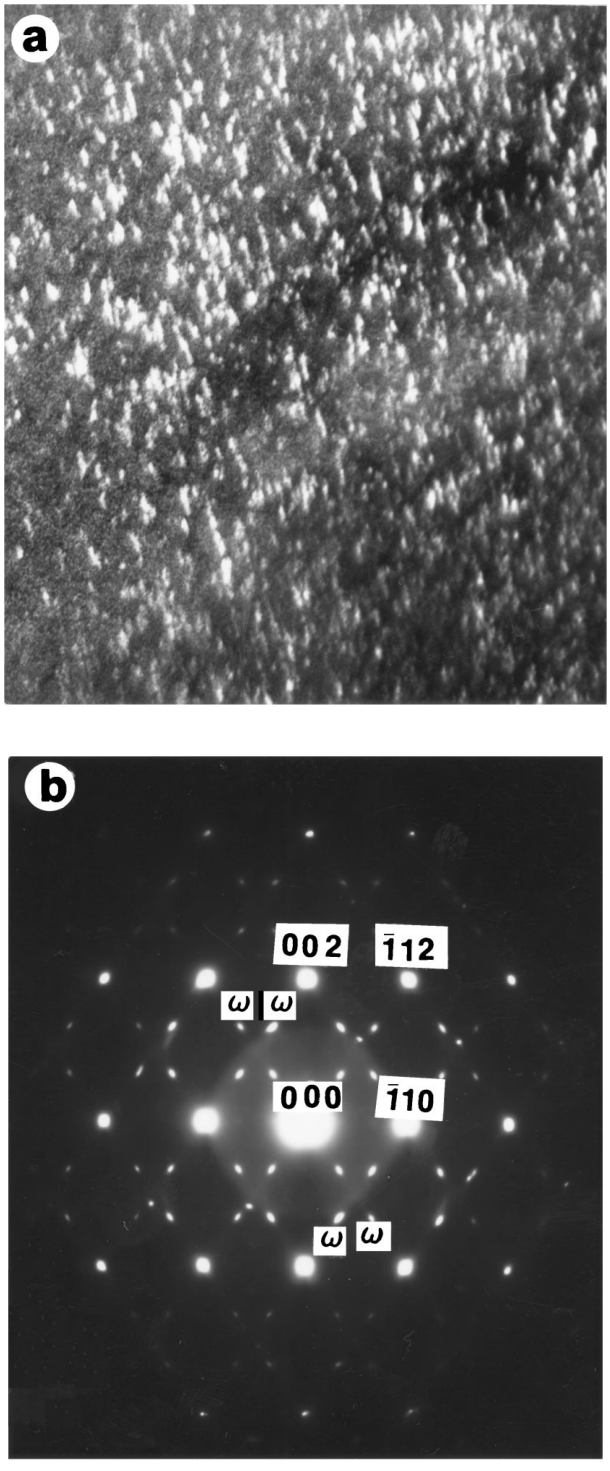

Figure 7 (a) Electron microscopic dark field image of the ω phase in the homogenized and furnace cooled TA6 alloy; (b) SAD pattern of the same sample, $g = [011]_\beta$.

TABLE IV Phases present in the solution treated alloys

Alloy	Analyzed content (wt%)	Phases present: Air cooled	Phases present: Water quenched
TA1	Ti-25.0Nb-21.9Ta	$\alpha+\beta+\omega_{iso}$	$\alpha''+\beta+\omega_{ath}$
TA2	Ti-23.2Nb-22.0Ta	$\alpha+\beta+\omega_{iso}$	$\alpha''+\beta+\omega_{ath}$
TA3	Ti-14.0Nb-37.6Ta	$\alpha+\beta+\omega_{iso}$	$\alpha''+\beta+\omega_{ath}$
TA4	Ti-12.7Nb-38.5Ta	$\alpha+\beta+\omega_{iso}$	$\alpha''+\beta+\omega_{ath}$
TA5	Ti-23.8Nb-21.6Ta-4.6Zr	$\alpha''+\beta+\omega_{ath}$	$\alpha''+\beta+\omega_{ath}$
TA6	Ti-22.2Nb-22.2Ta-4.1Zr	$\alpha''+\beta+\omega_{ath}$	$\alpha''+\beta+\omega_{ath}$
TA7	Ti-29.2Nb-12.4Ta-7.1Zr	$\beta+\omega_{ath}$	$\beta+\omega_{ath}$
TA8	Ti-35.5Nb-5.0Ta-6.9Zr	$\beta+\omega_{ath}$	$\beta+\omega_{ath}$
TA9	Ti-35.3Nb-5.7Ta-7.3Zr	$\beta+\omega_{ath}$	$\beta+\omega_{ath}$

4. Discussion

This investigation has shown that the phase transformations observed in Ti-Nb-Ta-(Zr) alloy are sensitive to both cooling rate and chemical composition. These observations can be considered by sub-dividing the alloys into three groups: (1) ternary alloys, (2) quaternary alloys containing approximately 4.1–4.6 wt% Zr and (3) quaternary alloys containing approximately 7 wt% Zr. Phases observed by optical microscopy, x-ray diffraction and transmission electron microscopy following solution treatment with different cooling conditions are summarized in Table IV. The transformation modes observed in this study can also be summarized in the form of schematic continuous cooling transformation (CCT) diagrams, Fig. 8. The position and shapes of these curves were drawn to elucidate the decomposition of the β phase during cooling from above the transus.

Fig. 8a shows that furnace cooling TA1 to TA4 involved intrusion into the $\beta+\alpha$ phase field. A similar transformation was also observed after air cooling with ω precipitation within the β phase occurring at lower temperatures. Since the $\beta \rightarrow \alpha$ transformation is accompanied by elemental partitioning, enrichment of the β phase occurs, the M_s of the retained β being suppressed below room temperature. Thus, no α' or α'' should be or was observed under these cooling conditions, in agreement with the microstructure shown in Figs 3 and 4. Faster cooling of TA1 through TA4 alloys from the β phase field, i.e., oil or water quenching did however result in partial transformation of the β phase to α'' martensite. In addition, these faster cooling rates suppressed ω_{iso} formation, ω_{ath} being observed within the β matrix. The suppression of ω_{iso} is most clearly shown by comparing the ω containing electron diffraction patterns following air (Fig. 4b) and water quenching (Fig. 2b). ω suppression in TA1 through TA4 is expected to lead to a reduction in microhardness, consistent with present results and those previously obtained in binary Ti-53.2 wt% Ta [10] and Ti-(45.4–51.1wt%) Nb [2] alloys.

In this study, ω has been designated as ω_{ath} and ω_{iso} according to their morphology and diffraction features. Athermal ω formation involves a displacive mechanism, that is, it occurs by collapse of the planes within the parent phase, β [11, 12]. Since no solute diffusion is necessary for ω_{ath} formation, it occurs as soon as the thermodynamic driving force is sufficient to initiate the plane collapse. Its formation does not therefore depend on cooling rate. Finally, due to the small lattice distortion associated with the displacive formation and its low percentage transformation, ω_{ath} is typically characterized by the diffuse streaking in electron diffraction patterns.

Alternatively, formation of isothermal ω, ω_{iso}, involves diffusion. Hence, it requires time and a temperature sufficient for solute redistribution in the matrix. Therefore, ω_{iso} is usually characterized by a

recognizable morphology, cuboidal or lenticular, with clear evidence of its formation in electron diffraction patterns. In the current study, ω_{iso} forms during slow continuous cooling, the slow cooling providing the necessary time at temperature for ω nucleation and growth. However, it is reasonable to assume that the precipitation kinetics of ω_{iso} will be accelerated by ω_{ath} below the ω_s temperature as shown by dashed part of the ω transformation curves in Fig. 8.

Addition of Zr to the ternary alloys increased the stability of the β phase in TA5 and TA6 alloys, displacing the $\beta \rightarrow \alpha$ transformation to increased times, Fig. 8b. The β phase was sufficiently stable that the $\beta \rightarrow \alpha$ transformation was avoided in all the cooling conditions employed in this investigation. The addition of Zr also decreased the Ms temperature and hence decreased the α'' volume fraction after water and oil quenching as seen for TA5 in Fig. 1b. At intermediate cooling rates, i.e., air cooling, only very diffuse diffraction streaking from ω_{ath} can be seen in SAD pattern. When furnace cooled, the M_s was further lowered by the precipitation of ω_{iso} and never reached, a microstructure of $\beta + \omega_{iso}$ being observed after the furnace cooling, Fig. 7. Previous study [9] supports the suggestion that precipitation of the ω phase results in the enrichment of β stabilizers in the matrix, hence increasing the stability of the β matrix and lowering the M_s.

Further increasing the Zr content, TA7 through TA9, continuously increased the stability of the β phase, no α'' martensite being observed after air cooling, i.e., the M_s temperature has decreased below room temperature. In agreement with the observation in TA5 and TA6, the addition of Zr also delayed isothermal ω formation in TA7 through TA9. Hence, after air cooling, ω_{iso} did not develop in the higher Zr containing quaternary alloys. The CCT curve for these alloys is shown in Fig. 8c. The presence of ω_{ath} rather than ω_{iso} with the addition of Zr is consistent with prior observations [13, 14]. In addition, the high content of Nb in TA7–TA9 may also have contributed to the stability of the β phase [2].

Finally, the suppression of ω with Zr addition in the quaternary alloys is also thought to be responsible for the decrease in dynamic modulus when these alloys are compared to the binary alloys containing similar amounts of Nb [15, 16]. The decrease in dynamic modulus accompanying suppression of ω is consistent with the modulus minima observed in binary Ti-Nb alloys at approximately 42 wt.% Nb [15, 16], i.e., close to the Nb content required for ω suppression. It has also been observed that the dynamic moduli of the quaternary alloys considered in this study appeared to have a minima at 5 at% Zr and a Nb/Ta ratio of 12.0. Although a complete rationale for this latter observation is presently unavailable, it is proposed that two effects may be contributing. The first involves the increased stability of β structure with respect to ω formation, the second is attributed to the preferred site occupancy of Nb, Ta and Zr within the bcc unit cell, its effect on the nature of bonding and thereby the minima in the modulus of elasticity remains to be investigated.

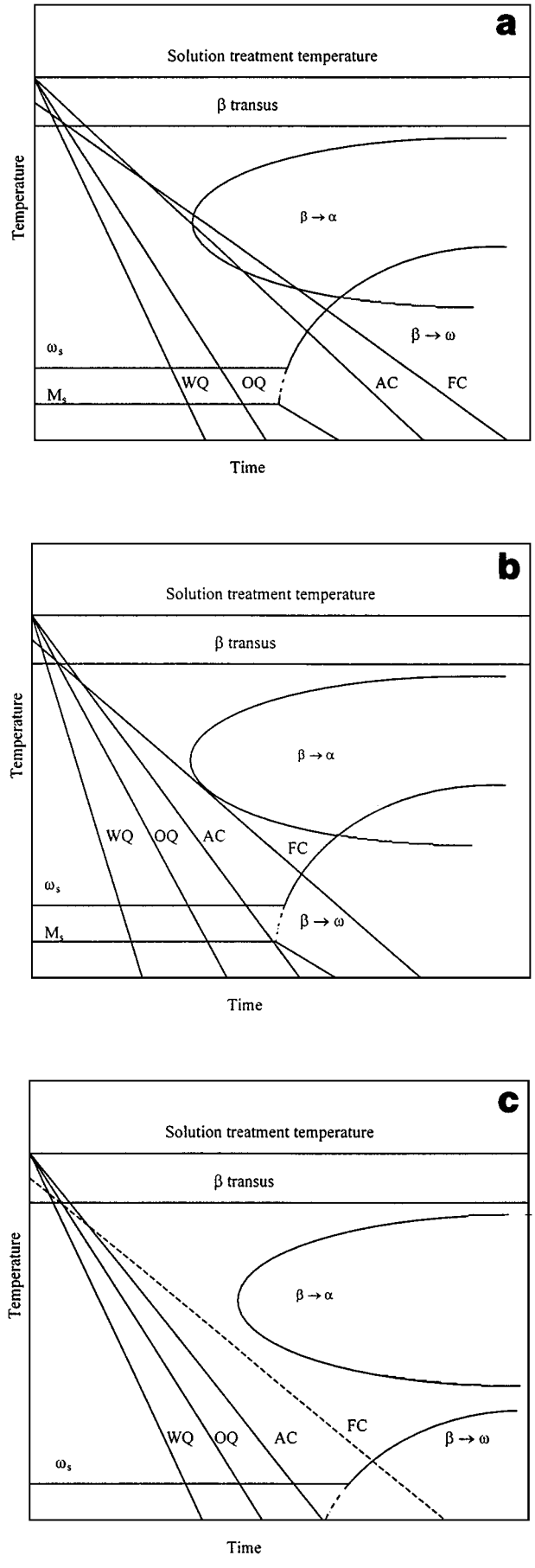

Figure 8 Schematic CCT diagrams for Ti-Nb-Ta and Ti-Nb-Ta-Zr alloys. (a) TA1–TA4, (b) TA5 and TA6, (c) TA7–TA9.

5. Conclusions

1) In ternary Ti-(13–26) Nb-(22–38) Ta (wt.%) alloy, water and oil quenching resulted in the formation of disordered orthorhombic martensite contained within a $\beta + \omega_{ath}$ matrix while increase of Nb + Ta resulted in decrease of the martensite. Air cooled alloys exhibited fine α and ω_{iso} within the β matrix.

2) Addition of 4.1–4.6 wt% Zr stabilizes the β phase, the $\beta \rightarrow \alpha$ transformation being completely suppressed in all the cooling conditions employed in this study. The $\alpha'' + \omega_{ath}$ microstructure within a retained β matrix was observed for cooling conditions faster than air cooling and the $\beta + \omega_{iso}$ after furnace cooling.

3) The rate of ω_{iso} formation was shown to be cooling rate dependent, the transformation being initiated by a displacive transformation. The addition of Zr retarded the development of ω_{iso} and resulted ω_{ath} formation in Zr containing alloys after air cooling.

4) Dynamic modulus determination of the air cooled quaternary alloys indicated that the dynamic modulus was sensitive to composition. A minima at Nb/Ta ratio of 12.0 and Zr content of 5 at% was observed.

Acknowledgements

The authors wish to thank Osteonics Corporation and Teledyne-ALLVAC for partial sponsorship of this research.

References

1. A. R. G. BROWN and K. S. JEPSON, *Mem. Sci. Rev. Metall.* **63** (1966) 575.
2. D. L. MOFFAT and D. C. LARBELIESTIER, *Metall. Trans.* **19A** (1988) 1677.
3. T. AHMED and H. J. RACK, *Journal of Materials Science*, in press.
4. N. Y. ALEKSEYEVSKIY, O. S. IVANOV, I. I. RAYEVSKIY and M. V. STEPANOV, *Fiz. Metal. Metalloved.* **23**(1) (1967) 28.
5. M. SUENAGA and K. M. RALLS, *J. Appl. Phys.* **40**(11) (1969) 4457.
6. E. M. SAVITSKII *et al.*, *Dokl. Akad. Nauk SSSR* **196**(5) (1971) 1145.
7. Kobe Steel Ltd., German Patent# 2350199, July 1974.
8. "Least Square Unit Cell Refinement", Program after Appleman and Evans (1973), implementation by R. G.
9. T. W. DUERIG, G. T. TERLINDE and J. C. WILLIAMS, *Met. Trans.* **11A** (1980) 1987.
10. K. A. BYWATER and J. W. CHRISTIAN, *Phil. Mag. A* **25** (1972) 1249.
11. D. DE FONTAINE, N. E. PATON and J. C. WILLIAMS, *Acta Metall.* **19** (1971) 1153.
12. D. DE FONTAINE and O. BUCK, *Philos. Mag.* **27** (1973) 967.
13. J. C. WILLIAMS, B. S. HICKMAN and D. H. LESLIE, *Metall. Trans.* **2** (1971) 477.
14. T. AHMED and H. J. RACK, unpublished research.
15. S. G. FEDOTOV and O. K. BELOUSOV, *Phys. Met. Metall. (USSR)* **17**(5) (1964) 83.
16. S. G. FEDOTOV, "Titanium Science and Technology," edited by R. I. Jaffee and H. M. Burte (Plenum Press, New York,) p. 871.

Received 10 February 1997
and accepted 15 July 1999